EUROPEAN ORGANIZATION FOR NUCLEAR RESEARCH

CERN-SL-98-018 (AP)

Transverse coupled-bunch instabilities for non-symmetric bunch fillings

O. Meincke

Abstract

A program has been written in order to investigate transverse coupled-bunch instabilities for non-symmetric bunch fillings in the case of a large number of bunches. After a short description of the method used to find the instability growth rates, first results of the program are discussed for the SPS and LHC. In particular, a systematic study of the effect of fluctuations in the bunch populations is presented.

Geneva, Switzerland

May 27, 1998

1 Introduction

The LHC will be operated with a total of 2835 bunches per beam, most of which having a longitudinal separation of 25 ns. The wake fields generated by a bunch in the vacuum chamber environment are likely to last long enough to affect the following bunches, potentially leading to coupled multi-bunch instabilities.

In order to decide whether the beam motion is stable or unstable, one usually solves the interaction matrix of the bunches for the complex eigenfrequencies. The imaginary parts of these frequencies give the damping constants for stable modes or the growth rates for unstable modes.

In the case of a symmetric bunch filling, i.e. a bunch filling in which the bunches are equally spaced and contain all the same number of particles, a closed expression for the eigenfrequencies can be found. For non-symmetric fillings in which the bunches are separated by gaps of different length or in which the bunch population varies among the bunches, no such general analytic solution exists. The latter filling scheme, however, is the more likely situation in reality. In the SPS as LHC injector, for example, the bunches will occupy only $\frac{3}{11}$ of the ring, and an LHC filling will consist of a total of 35 bunch trains separated by gaps of different length [1]. In order to investigate multi-bunch effects for non-symmetric fillings, a program has been written which calculates the wake field effects of the bunches on each other and solves numerically the interaction matrix for the complex eigenfrequencies. The program takes up the approach of the code MBI,[1] but it extends the latter in the way that not only resistive wall but also resonator and space charge impedances are used to model the transverse impedance of the ring. Moreover, the calculation of the resistive wall impedance allows for laminated beam pipe walls of finite thicknesses.

After a short introduction of the basic equations and assumptions, the different impedance classes which are used in the calculations are described. The remaining sections discuss the results of the program. Table 1 summarises the SPS and LHC machine parameters which have been used in the calculations [1, 2]. Note that the bunch intensities correspond to the *ultimate* LHC beam.

2 Basic equations

Throughout this paper, we consider transverse oscillations of M rigid bunches. The interaction between the bunches due to their wake fields is assumed to take place locally. The bunch motion is linear between the wake field kicks with all bunches having the same betatron frequency ω_β. The wake field effects are described in terms of the machine impedance. The lumped impedance is localised at the azimuth $\theta_Z = 0$.

[1]The multi-bunch beam instability simulation code MBI was written by N. V. Mityanina, BINP, Novosibirsk.

		SPS	LHC
Energy	GeV	26	450
Machine radius	m	1100	4242.89
Revolution frequency	Hz	43347.6	11245.5
vertical betatron tune		26.7	63.31
Number of bunches		243	2835
Particles per bunch		$1.7 \cdot 10^{11}$	$1.7 \cdot 10^{11}$
r.m.s. bunch length	ns	1	0.43
Transverse beam size (1σ)	mm	2.3	1.15
RF harmonic number		4620	35640

Table 1: Machine parameters of the SPS and LHC used in the calculations.

With these assumptions, the Fourier transform of the equation of motion of bunch j can be written as

$$(-\Omega^2 + \omega_\beta^2)\ \widetilde{y}_j = i\ \frac{\omega_\beta r_0 \beta}{\gamma T_0^2} \sum_{k=1}^{M} N_k\ \widehat{Z}_{jk}(\Omega)\ \widetilde{y}_k, \tag{1}$$

where $\widetilde{y}_j$ describes the oscillation amplitude of bunch j, r_0 is the classical particle radius and β denotes the β-function at the position of the wake field kick. γ is the relativistic energy factor and T_0 the revolution time of the bunches. The number of particles per bunch N_k can vary from bunch to bunch. The effective impedance $\widehat{Z}_{jk}(\Omega)$ is given by the expression

$$\widehat{Z}_{jk}(\Omega) = \sum_{p=-\infty}^{\infty} Z_\perp(\Omega + p\omega_0)\ |\widetilde{\rho}_0(\Omega + p\omega_0)|^2\ e^{i(\Omega + p\omega_0)t_{jk}}, \tag{2}$$

where $\omega_0 = 2\pi/T_0$ is the angular revolution frequency of the bunches, $Z_\perp(\omega)$ is the transverse impedance and $\widetilde{\rho}_0(\omega)$ stands for the longitudinal bunch spectrum of the rigid bunches which is related to the Fourier transform of the bunch shape. The explicit form of the bunch spectrum is given in section 7 where the results for two different bunch shapes are compared. Furthermore, $t_{jk} = t_j - t_k$ where t_j is given by the initial azimuthal position θ_j of bunch j: $\theta_j = \omega_0 t_j$. The time t_j can be written as $t_j = b_j T_0/h$ with b_j the bucket number of bunch j and h the rf harmonic number.

Note that the product $Z_\perp(\omega)\ |\widetilde{\rho}_0(\omega)|^2$ does not depend on the bunch number. In appendix A.1 it is shown that the exponential phase factor in Eq. (2) is a periodic function with period $\Lambda\omega_0$ for a certain Λ, $1 \le \Lambda \le h$, such that

$$e^{i(\omega + \Lambda\omega_0)t_{jk}} = e^{i\omega t_{jk}}.$$

Taking advantage of this periodicity, the computation of the summation in Eq. (2) can be speeded up significantly [3]. For a resonator impedance (see Eq. (4)), one

can find a closed expression for the sum [5]. The complete summation algorithm is described in appendix A.

In the case of a symmetric bunch filling, Eq. (1) can be solved analytically, yielding the complex frequency shifts [4]

$$\Omega_m - \omega_\beta = -i \, \frac{N r_0 \beta}{2\gamma T_0^2} \sum_{p=-\infty}^{\infty} Z_\perp(pM\omega_0 + \omega_m) \, |\widetilde{\rho}_0(pM\omega_0 + \omega_m)|^2, \tag{3}$$

where $\omega_m = m\omega_0 + \omega_\beta$ denotes the zero-current frequency of mode m.

3 Impedance model of the ring

The following subsections describe the different beam pipe structures which are used in the program to model the impedance of the machine.

Resonators

The modes of a resonator-like beam pipe structure are determined by their frequency ω_R, quality factor Q, and shunt impedance R_s. Given these parameters, the contribution of a single mode to the transverse impedance can be expressed by

$$Z_\perp(\omega) = \frac{\omega_R}{\omega} \, \frac{R_s}{1 + iQ(\frac{\omega_R}{\omega} - \frac{\omega}{\omega_R})}. \tag{4}$$

Each structure can have several modes described by different sets of parameters. The total resonator impedance is the sum over all modes.

In the LHC calculations presented here, the contributions from both the superconducting and the septum cavities as well as the contributions from the experimental chambers of CMS, Alice and Atlas have been included. The mode parameters can be found either in [6] or in the impedance data base [7].

Resistive wall

The transverse resistive wall impedance is calculated in two different ways. For a two-layer beam pipe, like in the LHC, and large ratios between beam pipe radius b and skin depth $\delta(\omega)$,[2] i.e. $b/\delta(\omega) \gg 1$, one can obtain an approximate expression for the transverse resistive wall impedance per unit length [6]

$$\frac{Z_\perp(\omega)}{L} = \frac{c\rho}{\pi\omega b^3} \sqrt{\frac{-i\mu_0\omega}{\rho}} \, \frac{\tanh\left(t\sqrt{-i\mu_0\omega/\rho}\right) + \sqrt{\rho'/\rho} \, \tanh\left(t'\sqrt{-i\mu_0\omega/\rho'}\right)}{1 + \sqrt{\rho'/\rho} \, \tanh\left(t\sqrt{-i\mu_0\omega/\rho}\right) \tanh\left(t'\sqrt{-i\mu_0\omega/\rho'}\right)}, \tag{5}$$

[2] The skin depth is defined by $\delta(\omega) = \sqrt{2\rho/\mu_0|\omega|}$.

	L/C	b (m)	ρ (Ω m)	t (m)	ρ' (Ω m)	t' (m)
SPS	1	0.025	$9 \cdot 10^{-7}$	$1.75 \cdot 10^{-3}$		
LHC	0.9	0.019	$1.8 \cdot 10^{-10}$	$5 \cdot 10^{-5}$	$5 \cdot 10^{-7}$	0.01
	0.1	0.019	$1.5 \cdot 10^{-8}$	0.002		

Table 2: Beam pipe parameters for the SPS and LHC. The SPS has a homogeneous vacuum chamber whereas the beam pipe of the LHC consists of a cold and a warm section with different parameters. The large thickness t' of the outer layer of the LHC beam screen includes the thickness of the cold bore and outer steel surroundings. It has been shown [8] that the gap between beam screen and outer surroundings is not seen by the wave propagating along the beam pipe wall. C is the ring circumference.

where ρ and t are the resistivity and the thickness of the inner layer, ρ' and t' the corresponding quantities of the outer layer, respectively. μ_0 is the permeability of free space and c the speed of light. The formula can also be used in the case of a single layer of finite thickness, i.e. for $t' = 0$, and in the limit of an infinitely thick beam pipe wall (skin depth $\ll$ wall thickness).

For values $b/\delta(\omega) \lesssim 1$, the approximation (5) gives wrong results. In these cases the algorithm described in [9] is used to calculate the resistive wall impedance. This method allows for a cylindrical beam pipe wall made of an arbitrary number of layers with different material constants, namely conductivity, permittivity and permeability. The algorithm also includes space charge effects. The steps to be performed in order to compute the impedance are summarised in appendix B. Table 2 shows the parameters of the SPS and LHC vacuum chamber [6, 10].

Space charge

The transverse space charge impedance is defined by [4]

$$Z_\perp(\omega) = i\frac{\mu_0 c R}{\gamma^2}\left(\frac{1}{a^2} - \frac{1}{b^2}\right), \tag{6}$$

where R denotes the machine radius and a is the beam radius. Note that (6) is not a proper impedance since it also depends on beam parameters.

The space charge impedance has to be added only if Eq. (5) is used to compute the resistive wall impedance. The other algorithm already includes this contribution.

4 Accuracy of the eigenfrequency computation

In the case of a nominally filled LHC ring, the program has to diagonalise a 2835×2835 matrix in order to find the complex eigenfrequencies of the beam which from the numerical point of view is a non-trivial task. The program uses

a subroutine from the NAG library which is already optimised to reduce the numerical errors [11]. In order to check the accuracy achieved by the subroutine for matrices of large dimensions, a symmetric bunch filling was considered since in that case the computed eigenfrequencies can be compared with the results of the analytical solution (see Eq. (3)). This has been done for the case of 2970 bunches.[3] The eigenvalues close to zero with imaginary frequency shifts of the order of $\pm 10^{-5}$ show the largest errors which reach up to a few per mil. However, the first 50 maximum, respectively minimum, eigenvalues have relative errors of the order of 10^{-10} or less. Since one is mainly interested in these values (the stability of the beam is determined by the maximum growth rate), the accuracy is sufficient to predict the stability behaviour of the beam.

5 Symmetric vs. non-symmetric bunch fillings

An exactly symmetric bunch filling is only an idealised case. In practice, the bunch population will vary from bunch to bunch. Furthermore, the bunches in the LHC will not be equally spaced. The different rise times of the injection and dump kickers in the LHC and of the extraction kickers in the pre-accelerators, the PS and the SPS, impose a filling scheme for the LHC in which the bunch trains are separated by gaps of different length. An analytical expression for the coupled-bunch growth rates, however, is known only for the case of symmetric fillings. Based on the result of D. Kohaupt [12], S. Berg [13] has shown that the maximum growth rate of a non-symmetrically filled ring is always smaller than that of the corresponding symmetric filling. The latter is obtained by adding bunches to the non-symmetric filling in such a way that the bunches in the resulting filling are equally spaced, and by setting the number of particles per bunch to the maximum one in the non-symmetric filling. This gives a conservative upper bound for the growth rates since the corresponding symmetric filling has an increased beam intensity. The program has been used to study the growth rates of non-symmetric fillings in detail. In the following two sections, we will separately discuss unequal bunch spacings and fluctuations in the bunch populations, at constant total beam current.

Unequal bunch spacing

The behaviour of the growth rate obtained for different bunch configurations depends on the actual impedance in the ring. First, we will consider an impedance with a limited bandwidth, as it is the case, for example, for resonators. Then, only a relatively small fraction of the beam spectrum overlaps with the impedance. For such an impedance, the maximum growth rates of two different bunch fillings were

[3] The nominal 2835 bunches cannot be distributed equally over the 35640 buckets in the LHC so that the next possible larger number of bunches has been taken.

compared, namely a filling with 231 bunches equally distributed over 4620 buckets and a single bunch train in which all bunches are placed in successive buckets. The growth rates were calculated for resonators with different resonant frequencies ω_R. The quality factor Q of the resonators was altered proportionally to ω_R so that the ratio ω_R/Q remained constant. Hence, the peaks of the impedance swept across the beam spectra without changing their width so that in each growth rate calculation, the same number of spectral lines contributed to the effective impedance. The resonant frequencies were taken to be equal to the betatron harmonics $(m+q)\omega_0$, where q is the fractional part of the tune and ω_0 the revolution frequency of the beam. Fig. 1 shows the results for a ratio $\omega_R/Q = \omega_0$.[4] Apart from the narrow dip, the growth rates of the symmetric filling are independent of the resonant frequency of the resonator. The growth rates of the bunch train, on the other side, oscillate. For increasing resonant frequency, they approach the value of the maximum growth rate of the symmetric filling.

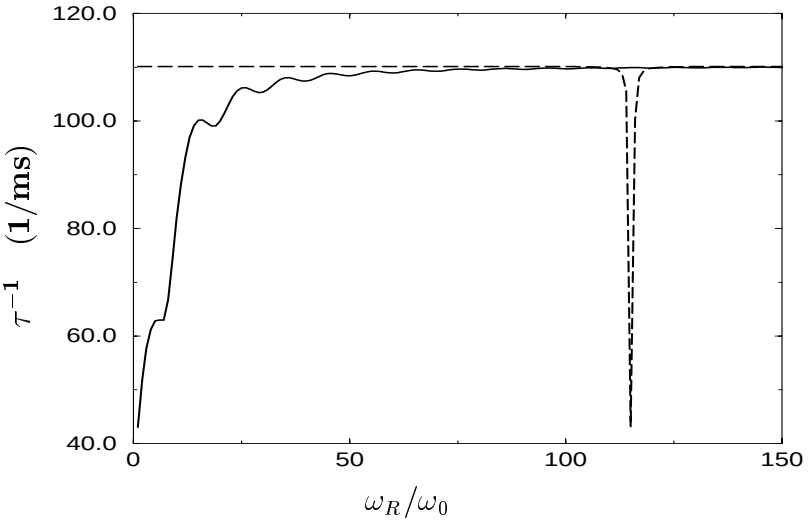

Figure 1: Maximum growth rate versus resonant frequency of a resonator-like impedance. The width of the impedance peaks were kept constant in the calculations. The upper curve shows the growth rates for 231 equally spaced bunches, the lower one corresponds to a bunch train containing the same number of bunches in successive buckets.

This different behaviour can be explained by looking at Fig. 2. Plotted is the real part of the resonator impedance together with the beam spectrum of the equal filling and the single bunch train, respectively. The former spectrum has lines only at the bunch frequency whereas the single bunch train generates additional lines at harmonics of the revolution frequency since it essentially corre-

[4]For the sake of simplicity, we neglect the influence of the bunch shape which would give additional suppression of the spectral lines at higher frequencies. This, however, affects both bunch fillings in the same way.

sponds to a rectangular current distribution. Negative frequencies in Fig. 2 lead to unstable coupled-bunch modes while the positive ones result in a stable beam motion. Therefore, the most unstable mode is found for a maximum overlap of the beam spectrum with the negative peak of the impedance. This case is illustrated in Fig. 2 for a resonator with resonance frequency $\omega_R = (20 + q)\omega_0$. Since we are only considering the maximum growth rates, the overlap of the spectrum with the negative peak is always largest and thus does not change for different resonant frequencies. Increasing the resonant frequency effectively shifts the positive peak of the impedance towards spectral lines at higher frequencies, thereby only changing the overlap of the spectrum with the positive peak. The cancellation between positive and negative frequency lines varies according to the shape of the beam spectrum which results in the growth rate modulations of the bunch train visible in Fig. 2. The sparse spectrum of the symmetric filling, on the other

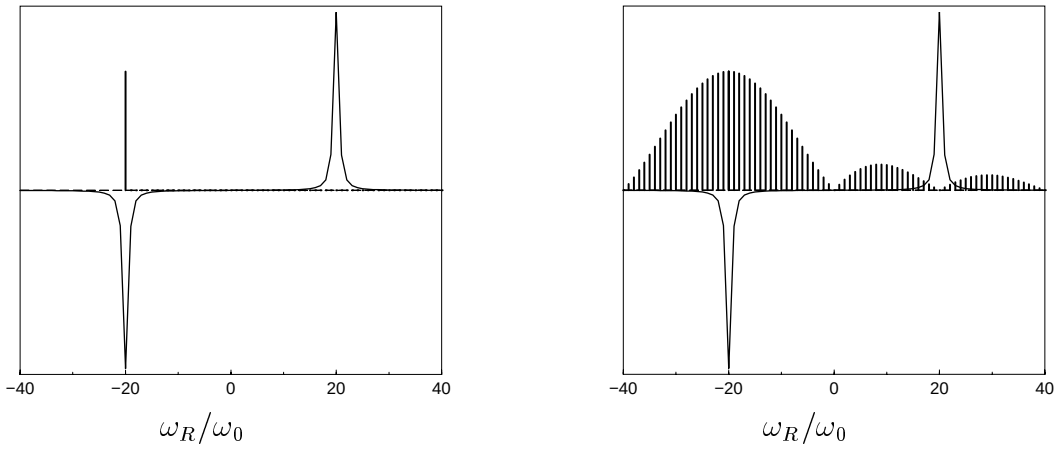

Figure 2: Real part of a resonator impedance with $\omega_R/Q = \omega_0$, $Q = 20$, together with the most unstable coupled-bunch mode spectra produced by 231 equally spaced bunches (left) and a bunch train (right). In the frequency range shown, the symmetric filling has only one spectral line.

side, has no frequency line falling into the bandwidth of the positive peak. Consequently, there is no cancellation between positive and negative lines so that the maximum growth rate remains unchanged when the resonant frequency of the resonator is increased. One observes a contribution from positive frequency lines only if the resonant frequency is about half the bunch frequency of the symmetric filling. This is just the frequency where the dip occurs in Fig. 1.[5]

[5]The fact that at the dip, the growth rate of the non-symmetric filling is larger than that of the symmetric filling does not violate Kohaupt's and Berg's criteria because their corresponding symmetric filling which gives the upper bound would consist of 4620 equally spaced bunches with a total beam current which is 20 times larger.

More precisely, if the resonant frequency differs from half the bunch frequency by more than the width of the impedance peaks, the spectral lines at positive frequencies do not contribute. In this case, the maximum growth rate of the equally spaced bunches is an upper bound for the growth rates of non-symmetric fillings with the same total beam current. In order to verify this behaviour, the growth rates of different bunch fillings have been computed. The bunch populations have been kept fixed but the azimuthal distribution of the bunches was varied. To that end, 231 bunches were randomly distributed over 4620 equally spaced bunch places. The resonant frequency of the resonator was chosen as $(114+q)\omega_0$ so that the first positive spectral line appears just at the edge of the positive peak of the impedance. Fig. 3 shows the maximum growth rates of 7500 random samples of different bunch configurations. The maximum growth rate of the symmetric filling, i.e. 231 equally spaced bunches, is $\tau^{-1} \approx 106\ \mathrm{s}^{-1}$. It is much larger than the growth rates of the non-symmetric fillings which scatter between $64\ \mathrm{s}^{-1}$ and $67\ \mathrm{s}^{-1}$.

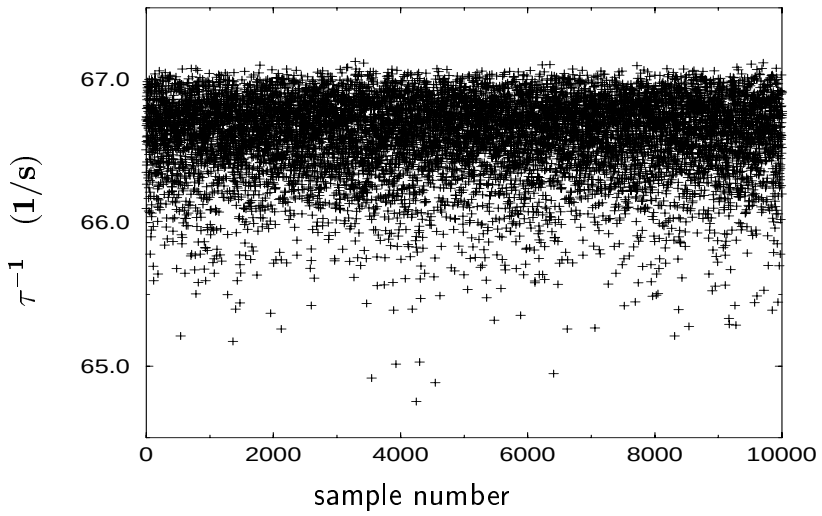

Figure 3: Maximum growth rates of different bunch configuration for a resonator impedance with resonant frequency $\omega_R = (114+q)\omega_0$ and quality factor $Q = 114+q$. For each calculation, 231 bunches were randomly distributed over 4620 bunch places.

The situation is different for a broad-band impedance, like the resistive wall impedance. In this case, the single bunch train has a larger growth rate compared to the symmetric filling because its spectrum has strong lines at low frequencies where the real part of the impedance is large. The equally spaced bunches, on the other side, sample the impedance at the bunch frequency so that the effective impedance is mainly determined by the lowest harmonic of the unstable coupled-bunch mode. This can be seen from Fig. 4 where the maximum growth rates of the symmetric filling and the bunch train are plotted as a function of the

fractional part of the tune. The growth rates were calculated for 231 bunches and SPS parameters for the resistive wall impedance (see Table 2). This time, the growth rates of the bunch train do not reflect the shape of the beam spectrum because virtually the whole spectrum overlaps with the real part of the impedance so that details of the spectrum cannot be resolved. Notice also the decrease of the growth rates for large fractional tunes $q \lesssim 1$. For these tunes, the first spectral line at negative frequency has a very small frequency. The skin depth, then, becomes much larger than the thickness of the beam pipe wall so that the wake fields largely leak out of the beam pipe without interacting with the following particles. Consequently, the impedance decreases at low frequencies.

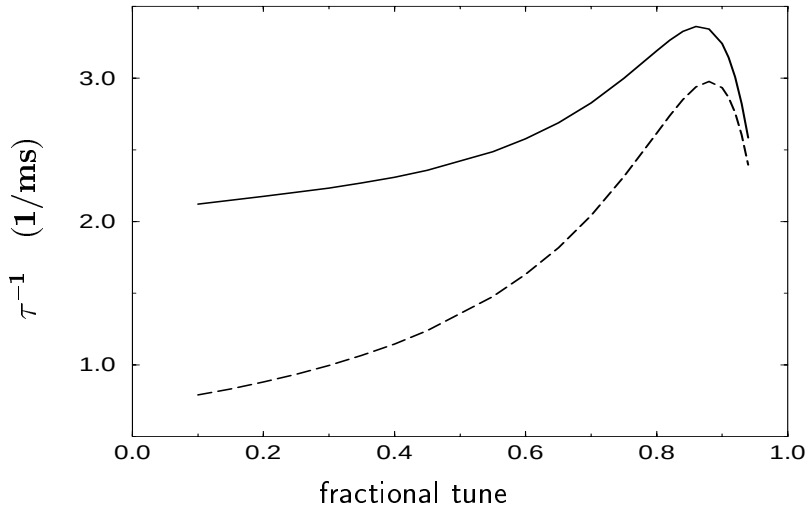

Figure 4: Maximum growth rates as a function of the fractional tune. Two bunch fillings are compared, namely 231 equally spaced bunches (dashed line) and a single bunch train in which the bunches fill successive buckets (solid line).

The fact that for a resistive wall impedance, more symmetric fillings have smaller growth rates will again be found in section 6 where different injection schemes for the SPS and LHC are compared. It will be shown that a symmetric injection is more favourable in terms of coupled-bunch instabilities.

In order to show that for the resistive wall impedance, the growth rate of the bunch train is an upper limit, the growth rates of randomly distributed bunches have been calculated as before, this time however for the resistive wall impedance in the SPS. Fig. 5 shows the maximum growth rates of 10000 different bunch fillings. All values are well below the maximum growth rate of the bunch train which in this case is $\tau^{-1} \approx 2.8$ 1/ms.

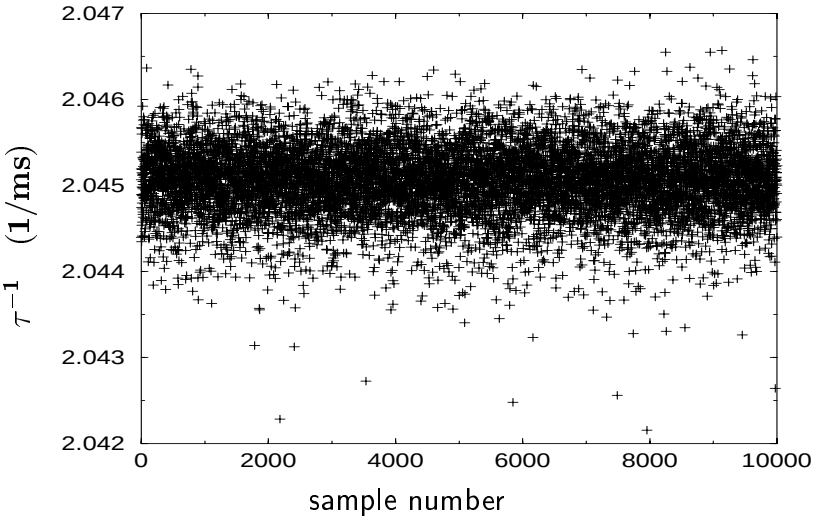

Figure 5: Maximum growth rates of different bunch configurations for the resistive wall impedance in the SPS. For each calculation, 231 bunches were randomly distributed over 4620 equally spaced bunch places.

Fluctuations in the bunch populations

In case the bunch population varies from bunch to bunch, the effect of the impedance due space charge and image current becomes important [14]. This impedance is purely imaginary and therefore causes a real frequency shift of the bunch oscillation frequencies. The corresponding wake field is local to the bunches so that they act only on themselves. Since the wake fields are intensity dependent, this interaction results in a frequency spread which is proportional to the spread in the bunch populations. The additional frequency spread decouples, at least partly, the motion of the bunches and thus tends to stabilise the beam. This effect is similar to the mechanism of Landau damping, however, we will see that the frequency spread has to be much larger than the growth rate itself in order to obtain an appreciable damping effect whereas in the case of Landau damping, they only have to be of comparable size. The space charge impedance, of course, is also present in the case of equal bunch populations, however, it does not lead to a spread in oscillation frequencies because in that case all bunches experience the same frequency shift.

In order to illustrate this stabilising effect, we consider 231 equally spaced bunches with bunch intensities which increase linearly along the beam. This yields a rectangular distribution in tunes. In Fig. 6, the maximum growth rates are plotted as a function of the relative spread in the bunch population. The growth rates were computed for the resistive wall impedance in the SPS (see Table 2), although the effect of stabilisation is independent of the actual impedance. The dashed lines in Fig. 6 show the frequency spreads induced by space charge and

image currents. The lower dashed line is the same as the upper one, but scaled by a factor of 0.1. One can see that the growth rates decrease with increasing spread in the bunch oscillation frequencies. However, for a significant reduction of the growth rate, the frequency spread has to be much larger than the growth rate itself. For example, to halve the largest growth rate in Fig. 6, one needs a frequency spread which is more than two times larger.

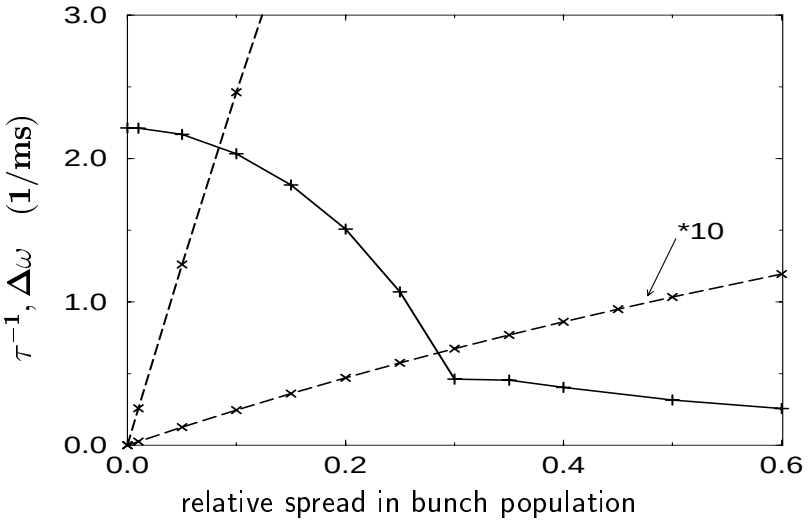

Figure 6: Growth rate τ^{-1} versus relative spread in bunch population in the SPS at injection (solid line). The dashed lines show the frequency spread $\Delta\omega$ induced by space charge and image currents. The values of the lower line have to be multiplied by a factor of 10 in order to obtain the real spread.

Next, the space charge effect has been investigated for more realistic situations. To that end, 231 equally spaced bunches were considered with randomly fluctuating bunch populations. The bunch populations were normalised such that the total number of particles in the beam was constant. Again, the growth rates were calculated for different spreads in the bunch populations. For each spread, the maximum growth rates of 1000 random samples of bunch fillings with different bunch populations have been averaged. The growth rates were computed for SPS parameters at injection (see Table 1). Fig. 7 shows the averages together with their standard deviations (solid line). For comparison, the growth rates for the linear increase in bunch population are also plotted (dashed line). The two curves show qualitatively the same behaviour which indicate that mainly the total frequency spread is important for the stabilisation regardless of how the frequencies vary from bunch to bunch.

However, the effect is relatively small in the SPS and LHC. The beams available in the SPS under normal operation conditions have fluctuations in the bunch populations usually of the order of 5 - 10% [15]. Such a spread would reduce the

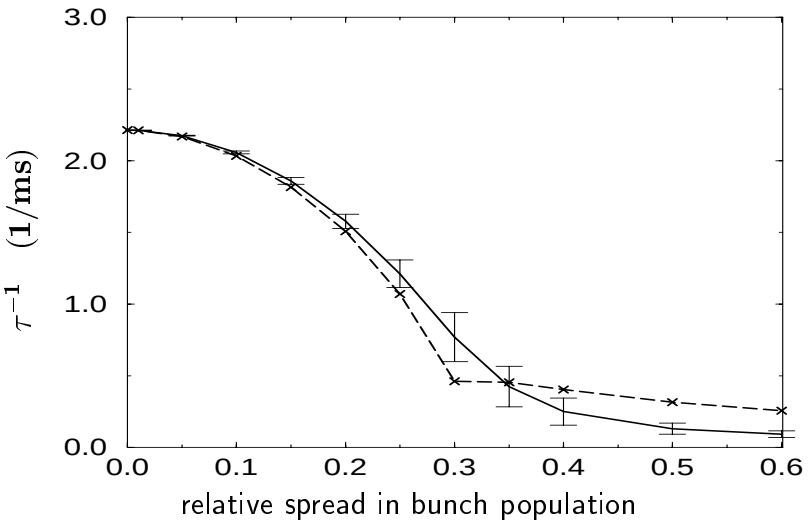

Figure 7: Growth rate τ^{-1} versus relative spread in bunch population in the SPS at injection. The solid curve shows the average growth rates and their standard deviations in the case of randomly fluctuating bunch populations. For comparison, also the growth rates for a linear increase in bunch population are plotted (dashed curve).

growth rates in the SPS at injection by only less than 10%. On the other side, the results discussed so far have been obtained for a simple impedance model of the SPS (only resistive wall and space charge impedance). Using a better description of the ring, one may find a larger stabilising effect although calculations have shown that the pumping ports and cavities do not give additional damping. In the LHC, the effect is even smaller than in the SPS. Due to the higher beam energy, the space charge induced frequency spread is negligible compared to the growth rate of coupled-bunch instability.

The numerical calculations so far indicate that depending on the impedance, one can give upper bounds for the growth rates of non-symmetric bunch fillings which are less conservative than the criteria found by Kohaupt and Berg. In addition, a spread in bunch population which in reality is always present tends to stabilise the beam motion. Growth rates obtained for uniform bunch populations therefore represent the worst case.

6 Growth rates during injection

In this section the effect of different filling schemes on the instability growth rates during injection is discussed. We compare the growth rates for a consecutive injection with those for a symmetric one. In a consecutive injection the newly injected bunch train is placed just behind the already circulating bunches whereas in a symmetric injection it is tried to keep the filling at each injection step as

symmetric as possible.

LHC

In order to fill one ring of the LHC, the SPS has to deliver 12 bunch trains. Each train consists of 243 bunches except the last one which contains only 162 bunches in order to provide a sufficiently large gap for the rise time of dump kicker. The sequencing of the injected bunch trains for both schemes is illustrated in Fig. 8.

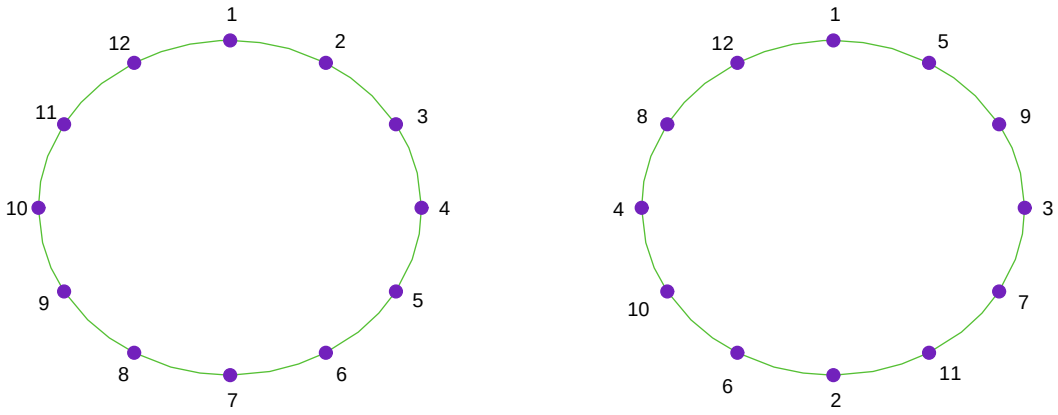

Figure 8: Sequence of the injected bunch trains in the case of a consecutive (left) and a symmetric (right) injection in the LHC for the nominal number of bunch trains. The dots show the bunch train position and the assigned numbers indicate the injection sequence.

Fig. 9 compares the growth rates during injection for a nominal LHC filling of 2835 bunches. One can see that the growth rates for the symmetric injection are somewhat smaller than those for the consecutive case. However, the largest growth rate is found for the fully filled ring and thus it is the same in both cases, namely $\tau^{-1} \approx 37.2\ \frac{1}{\mathrm{s}}$. The growth rates are entirely determined by the resistive wall impedance, the higher order modes of the resonator impedances give only a small contribution. Concerning coupled-bunch instabilities there is no advantage in using a symmetric filling scheme for the LHC.

SPS

The same study has been done for the SPS as LHC injector. In the nominal filling scheme, three bunch trains (each containing 81 bunches) are injected one behind the other. The resulting filling occupies only a third of the ring circumference. The growth rates for this scheme were compared with the growth rates for a symmetric injection in which the three bunch trains are separated by equal gaps. In the calculation, only the resistive wall and space charge impedance has been

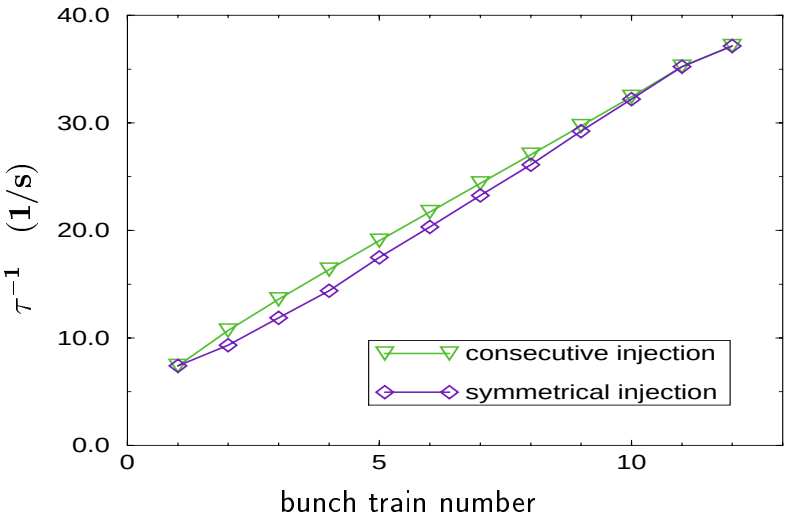

Figure 9: Instability growth rates in the LHC during injection using a consecutive resp. symmetric filling scheme.

taken into account. Fig. 10 shows the result. The differences in the growth rates for the different injection schemes is negligible ($< 0.5\%$). The growth rate for the nominally filled SPS (243 bunches) is $\tau^{-1} \approx 2.2\ \frac{1}{\mathrm{ms}}$. The estimates for the growth rate of the resistive wall instability in [10] agree with this result within a few tenth of a percent[6] although the calculation there did not include space charge effects.

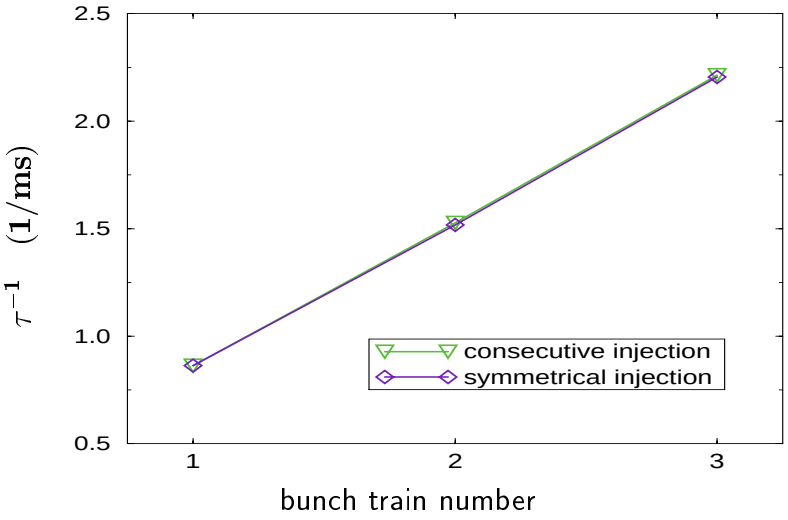

Figure 10: Growth rates in the SPS during injection for two different filling schemes.

[6]When the same transverse tune as in [10] is used, namely $Q_y = 26.6$.

7 Effect of different bunch shapes

From Eq. (1) it can be seen that the growth rates depend through the bunch spectrum $\widetilde{\rho}_0(\omega)$ on the longitudinal shape of the bunches. To see how strong this dependence actually is, two different bunch shapes have been used in the computation of the growth rates, namely a Gaussian and a cosine-squared shape. The Gaussian distribution with r.m.s. length σ_z is given by

$$\rho_0(z) = \frac{1}{\sqrt{2\pi}\sigma_z} e^{-z^2/2\sigma_z^2},$$

where z denotes the distance from the bunch centre. The cosine-squared distribution is defined by

$$\rho_0(z) = \frac{1}{\Delta}\cos^2(\pi\frac{z}{\Delta}) \qquad \text{for} \quad |z| \leq \Delta.$$

Outside the interval Δ: $\rho_0(z) \equiv 0$. The half base length Δ is chosen such that the distribution has a given r.m.s. length σ_z. Unlike the Gaussian shape, the cosine-squared shape does not extend to infinity. It is similar to a parabolic distribution but has the advantage that the derivatives at the edge of the distribution at $\pm\Delta$ are continuous. Such a bunch shape certainly describes the proton bunches in the LHC better than a Gaussian or parabolic one. The two bunch distributions are plotted in Fig. 11. Their bunch spectra are given by

$$\widetilde{\rho}_0(\omega) = e^{-\sigma_z^2\omega^2/2}$$

for the Gaussian distribution, and by

$$\widetilde{\rho}_0(\omega) = \frac{\sin(\omega\Delta/2)}{\omega\Delta/2} \, \frac{1}{1-(\frac{\omega\Delta}{2\pi})^2}$$

for the cosine-squared distribution.

However, it was found that for the impedance model used in the calculations the change of the bunch shape hardly effects the growth rates. The relative difference in the growth rates is only of the order of 10^{-6}.

8 Growth rates for doubled bunch spacing in the LHC

In order to avoid the electron-cloud instability, F. Ruggiero suggested to double the bunch spacing in the LHC and accordingly to increase the single bunch current in both LHC beams by a factor $\sqrt{2}$ to obtain the same luminosity. Here, we discuss the impact of these changes on the growth rates of coupled-bunch instabilities. To that end, every second bunch in the nominal bunch trains was taken out, leaving a total of 1435 bunches separated by 50 ns gaps within the bunch

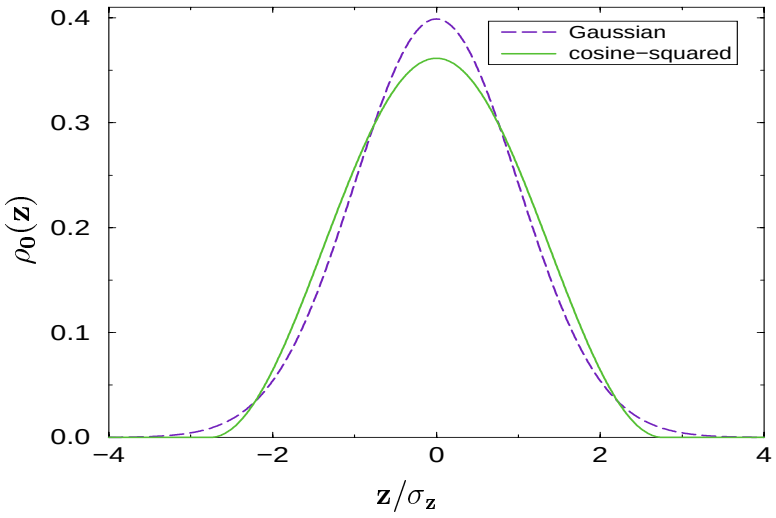

Figure 11: The Gaussian and cosine-squared bunch shapes used in the calculations.

trains. The separations between the individual bunch trains remained unchanged since they are already larger than 50 ns. In Fig. 12, the growth rates are plotted for different single bunch currents. For a fixed number of bunches, the growth rate increases linearly with the bunch current. The dashed line correspond to the single bunch current which yields the same luminosity as the nominal case. The growth rate for this current is $\tau^{-1} \approx 26.6\ \frac{1}{\mathrm{s}}$ to be compared with $\tau^{-1} \approx 37.2\ \frac{1}{\mathrm{s}}$ in the case of nominal bunch spacing and current. Notice that the growth rate scales with the total beam current rather than the single bunch current. For instance, in going from the nominal setup to the one with double bunch spacing but same luminosity, the total beam current is decreased by a factor of $\frac{1}{2835}\sqrt{2}$ which is roughly the ratio between the two corresponding growth rates. Thus, concerning the growth rates of coupled-bunch instabilities, the doubled bunch separation is preferable. Even if the single bunch current is raised up to the threshold current for the mode-coupling instability, i.e. $I_b \approx 0.57$ mA [6], the growth rate will not exceed the value obtained for the nominal parameters.

9 Conclusions

A program has been written in order to investigate transverse coupled-bunch instabilities for non-symmetric bunch fillings in the case of a large number of bunches. The accuracy of the numerical computation of the growth rates is very good. Comparison with the theoretical predictions for symmetric bunch fillings showed that the relative errors on the growth rates of the most unstable modes is of the order of 10^{-10} or less.

Depending on the impedance, upper bounds for the growth rates of non-

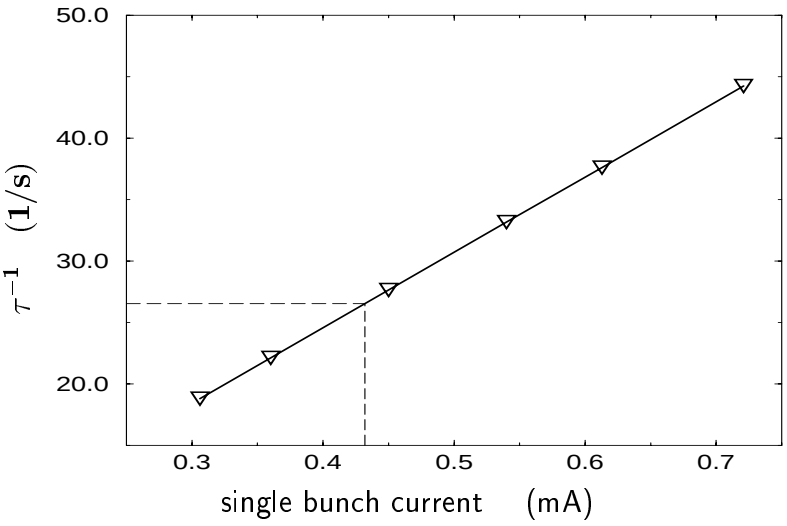

Figure 12: Coupled-bunch growth rate versus single bunch current for a 50 ns bunch spacing within the bunch trains in the LHC. The dashed line corresponds to the current which yields the same luminosity as the nominal values for bunch current and separation.

symmetric fillings have been given which are less conservative than the existing criteria. In addition, it has been shown that a spread in bunch populations helps to stabilise the beam motion.

Two different injection schemes for the SPS and LHC have been compared, namely a consecutive and a symmetric injection. In both cases, the growth rates during the symmetric injection are smaller than those of the consecutive injection. The largest growth rate, however, was found for the fully filled ring and therefore it is the same for both schemes. Concerning the growth rates of coupled-bunch instabilities, there is no significant advantage with a symmetric injection.

Doubling the bunch separation and increasing accordingly the single bunch current by a factor $\sqrt{2}$, which was suggested to avoid the electron-cloud instability, has also a beneficial effect on the coupled-bunch instabilities. The growth rate for a completely filled LHC at injection is lowered by about 30% with respect to the growth rate obtained for the nominal bunch currents and separations.

Acknowledgement

I would like to thank Francesco Ruggiero for many fruitful discussions and for carefully reading the manuscript. Thanks to J. Scott Berg and Luc Vos for their valuable suggestions and comments.

References

[1] The LHC Study Group, "The Large Hardron Collider, conceptual design", CERN AC 95-05 (LHC), (1995).

[2] "The SPS as injector for LHC, conceptual design", CERN SL 97-07 (DI), (1997).

[3] J. S. Berg, private communication, August 1997.

[4] A. Chao, "Physics of collective beam instabilities in high energy accelerators", John Wiley & Sons, Inc., (1993).

[5] K. Balewski, R. D. Kohaupt, "Analytic Evaluation of the Effective Impedance for Coupled Bunch Instabilities", DESY 90-152, (1990).

[6] J. S. Berg, "Transverse Instabilities in the LHC", LHC Project Report 16, (1996).

[7] O. Brüning, "ZBASE User's Guide Version 1.1, An Impedance Data Base Program", CERN SL 96-69 (AP), (1996).

[8] M. M. Karlinger, N. V. Mityanina, B. Z. Persov, V. P. Yakovlev, "LHC beam screen design report", Preprint BINP 94-45, (1994).

[9] B. Zotter, "Transverse oscillations of a relativistic particle beam in a laminated vacuum chamber", CERN 69-15 Rev., (1969).

[10] L. Vos, "Damping of coherent oscillations", CERN SL 96-66 (AP).

[11] "The NAG Fortran Library Manual, Mark 15", NAG Ltd, 1991.

[12] R. D. Kohaupt, "On Multi-Bunch Instabilities for Fractionally Filled Rings", DESY 85-139, (1985).

[13] J. S. Berg, "Bounds on multibunch growth rates when the bunch currents are not identical", CERN SL Note 97-72 (AP), (1997).

[14] E. D. Courant, A. M. Sessler, "Transverse coherent resistive instabilities of azimuthally bunched beams in particle accelerators", Rev. Sci. Instr., Volume 37, Number 11, (1966)

[15] W. Höfle, private communication, February 1998.

A Summation of the effective impedance

A.1 Periodicity of the exponential factor

Here, we will show that the exponential phase factor $e^{i\varphi_{jk}(\omega)}$ with $\varphi_{jk}(\omega) = \omega t_{jk}$ is periodic in ω with a period $\Lambda\omega_0$ for a certain Λ, $1 \leq \Lambda \leq h$. For the definitions of the symbols see section 2.

Let's designate by d the greatest common divider of all bunch separations so that $b_j - b_k = n_{jk}\, d$ with integer numbers n_{jk}. Then it exists an integer Λ, $1 \leq \Lambda \leq h$, so that $h = \Lambda\, d$.
Now, one can write

$$\varphi_{jk}(\omega) = \omega t_{jk} = \omega T_0 (b_j - b_k)/h = \omega T_0 n_{jk} d/\Lambda d = \omega T_0 n_{jk}/\Lambda.$$

Hence it follows for each $\varphi_{jk}(\omega)$ that

$$\varphi_{jk}(\omega + \Lambda\omega_0) = (\omega + \Lambda\omega_0) T_0 n_{jk}/\Lambda = \varphi_{jk}(\omega) + 2\pi n_{jk}$$

and

$$e^{i\varphi_{jk}(\omega + \Lambda\omega_0)} = e^{i\varphi_{jk}(\omega)}.$$

This periodicity can be used to speed up the computation of the effective impedance. To that end, we rewrite the infinite sum over p in Eq. (2) as a double sum. Setting $\Omega_p = \Omega + p\omega_0$, we can write

$$\sum_{p=-\infty}^{\infty} Z_\perp(\Omega_p)\; |\widetilde{\rho}_0(\Omega_p)|^2\; e^{i\Omega_p t_{jk}} = \sum_{m=0}^{\Lambda-1} e^{i\Omega_m t_{jk}} \sum_{\ell=-\infty}^{\infty} Z_\perp(\Omega_m + \ell\Lambda\omega_0)\; |\widetilde{\rho}_0(\Omega_m + \ell\Lambda\omega_0)|^2 \tag{7}$$

where we have made use of the periodicity in the exponential factor.

The infinite sums over ℓ (for different values of m) do not depend on the bunch number. They are performed only once and then stored. For the calculation of the matrix elements which are determined by the bunch separation between two bunches only the finite sums over m have to be computed. The advantage is that the infinite sum of the product $Z_\perp(\omega)\; |\widetilde{\rho}_0(\omega)|^2$ which in general involves time-consuming evaluations of complex elementary functions (like exp, cos, sin, ...) has to be done only once. On the other side, the summations needed to compute the different matrix elements, which in the case of a large number of bunches M are performed many, i.e. M^2, times are executed very fast since they run only over a few (of the order of M) summands. The largest gain in computing time is obtained in the case of a nearly equally filled ring with occasionally empty bunch places such that the number of empty bunch places is much smaller than the number of filled bunch places. This is true for the nominal bunch filling in the LHC.

A.2 Impedance sum of a resonator

Here, a closed analytical expression for the infinite sum in Eq. (7) in the case of a resonator-like beam pipe structure is derived. The argumentation follows mainly [5].
First, we write the sum in the following way:

$$\begin{aligned} S(\Omega) &= \sum_{\ell=-\infty}^{\infty} Z_\perp(\Omega_m + \ell\Lambda\omega_0)\ |\widetilde{\rho}_0(\Omega_m + \ell\Lambda\omega_0)|^2 \\ &= \int_{-\infty}^{\infty} d\omega \sum_{\ell=-\infty}^{\infty} \delta(\omega - (\Omega + \ell\Lambda\omega_0))\ Z_\perp(\omega)\ |\widetilde{\rho}_0(\omega)|^2. \end{aligned} \tag{8}$$

Inserting the Fourier series of the periodic δ-function

$$\sum_{\ell=-\infty}^{\infty} \delta(\omega - (\Omega + \ell\Lambda\omega_0)) = \frac{1}{\Lambda\omega_0} \sum_{k=-\infty}^{\infty} e^{ik(\omega-\Omega)T_0/\Lambda} \tag{9}$$

yields

$$S(\Omega) = \frac{1}{\Lambda\omega_0} \sum_{k=-\infty}^{\infty} \int_{-\infty}^{\infty} d\omega\ Z_\perp(\omega)\ |\widetilde{\rho}_0(\omega)|^2\ e^{ik\omega T_0/\Lambda}\ e^{-ik\Omega T_0/\Lambda}. \tag{10}$$

The resonator impedance (4) can be written in the form

$$Z_\perp(\omega) = -i\frac{\omega_R R_s}{\sqrt{4Q^2-1}} \left\{ \frac{1}{\omega - \omega_+} - \frac{1}{\omega - \omega_-} \right\} \tag{11}$$

where

$$\omega_\pm = -i\alpha \pm \sqrt{\omega_R^2 - \alpha^2} \quad \text{with} \quad \alpha = \frac{\omega_R}{2Q}.$$

Substituting Eq. (11) into Eq. (10) gives

$$\begin{aligned} S(\Omega) &= -i\frac{1}{\Lambda\omega_0}\frac{\omega_R R_s}{\sqrt{4Q^2-1}} \sum_{k=-\infty}^{\infty} e^{-ik\Omega T_0/\Lambda} \\ &\quad \int_{-\infty}^{\infty} d\omega\ |\widetilde{\rho}_0(\omega)|^2\ e^{ik\omega T_0/\Lambda} \left\{ \frac{1}{\omega - \omega_+} - \frac{1}{\omega - \omega_-} \right\}. \end{aligned} \tag{12}$$

The integral over ω can be performed using Cauchy's residue theorem. For $k > 0$ one has to close the integration contour in the upper ω-plane where the integrand is an analytical function.[7] Thus the integral is zero. For $k \leq 0$ the integration path is closed in the lower ω-plane where the residua of the two poles contribute to the integral. After some algebra, Eq. (12) reads

$$S(\Omega) = \frac{2\pi}{\Lambda\omega_0}\frac{\omega_R R_s}{\sqrt{4Q^2-1}} \sum_{k=0}^{\infty} \left\{ |\widetilde{\rho}_0(\omega_+)|^2\ e^{-ik(\omega_+ - \Omega)T_0/\Lambda} - |\widetilde{\rho}_0(\omega_-)|^2\ e^{-ik(\omega_- - \Omega)T_0/\Lambda} \right\} \tag{13}$$

[7] We assume that the bunch spectrum $\widetilde{\rho}_0(\omega)$ has no singularities which is true for physical bunch shapes.

The sums in this expression can be written in closed form:

$$\sum_{k=0}^{\infty} e^{-ik(\omega_{\pm}-\Omega)T_0/\Lambda} = \frac{1}{1-e^{-i(\omega_{\pm}-\Omega)T_0/\Lambda}} \tag{14}$$

so that finally

$$S(\Omega) = \frac{2\pi}{\Lambda\omega_0}\frac{\omega_R R_s}{\sqrt{4Q^2-1}}\left\{\frac{|\widetilde{\rho}_0(\omega_+)|^2}{1-e^{-i(\omega_+-\Omega)T_0/\Lambda}} - \frac{|\widetilde{\rho}_0(\omega_-)|^2}{1-e^{-i(\omega_--\Omega)T_0/\Lambda}}\right\}. \tag{15}$$

B Calculation of the transverse resistive wall impedance for a laminated beam pipe wall

The algorithm described here calculates the transverse resistive wall impedance for a cylindrical beam pipe. The beam pipe wall can consist of an arbitrary number of layers with different material constants: conductivity σ, permittivity ϵ and permeability μ. The calculation allows for beam velocities $v < c$ and it distinguishes between the velocities of the beam and the waves which are excited in the vacuum chamber. The boundary conditions outside the beam pipe can be defined either at infinity or for a perfect conductor or magnet at a finite radius. As driving source a continuous cylindrical beam is assumed which oscillates vertically. The derivation and detailed information can be found in [9].

The beam pipe cross section is divided into ring-like regions with different properties. The innermost region corresponds to the area occupied by the beam, the following region is the ring limited by the beam radius and the pipe radius, and so on. The regions are numbered beginning in the innermost one. The outer radius of the i-th region will be denoted by a_i.
The algorithm uses the following parameters:

Beam energy	γ_0
Machine radius	R
Tune	Q
Mode number	n
Beam velocity	$\beta_0 = \sqrt{1-\gamma_0^{-2}}$
oscillation frequency	$\omega = (n+Q)\beta_0 c/R$
Phase velocity	$\beta = (1+Q/n)\beta_0$
Wave number	k = n / R
Energy factor of the wave	$\gamma = 1/\sqrt{1-\beta^2}$

The algorithm performs successively the following steps, starting in the outermost region and going inwards:
(1) Calculate for each region i

- the complex dielectric constant $\tilde{\epsilon_i} = \epsilon_i + \mathrm{i}\frac{\sigma_i}{\omega\epsilon_0}$.
- the radial propagation constant $\nu_i = k\sqrt{1 - \mu_i\tilde{\epsilon_i}\beta^2}$.
- the coefficients R_i, R_i', S_i and S_i' (only for $i \geq 2$):

$$\begin{aligned} R_i &= K_1(\nu_i a_i)I_1(\nu_i a_{i-1}) - K_1(\nu_i a_{i-1})I_1(\nu_i a_i) \\ R_i' &= K_1(\nu_i a_i)I_1'(\nu_i a_{i-1}) - K_1'(\nu_i a_{i-1})I_1(\nu_i a_i) \\ S_i &= K_1'(\nu_i a_i)I_1(\nu_i a_{i-1}) - K_1(\nu_i a_{i-1})I_1'(\nu_i a_i) \\ S_i' &= K_1'(\nu_i a_i)I_1'(\nu_i a_{i-1}) - K_1'(\nu_i a_{i-1})I_1'(\nu_i a_i) \end{aligned}$$

  where $I_1(z)$ and $K_1(z)$ are modified Bessel-functions of first and second kind. The prime denotes the derivative with respect to the complete argument.

(2) The boundary conditions in the outermost region j determine the initial values of the coefficients $M_{kl}^{(j)}$ which are the starting point of the calculation (see below). They are

- for region j extending to infinity:

$$M_{11}^{(j)} = M_{22}^{(j)} = \left.\frac{K_1'}{K_1}\right|_{\nu_j a_{j-1}}.$$

- for region j bounded by a perfect conductor:

$$M_{11}^{(j)} = \frac{R_j'}{R_j} \quad \text{and} \quad M_{22}^{(j)} = \frac{S_j'}{S_j}.$$

- for region j bounded by a perfect magnet:

$$M_{11}^{(j)} = \frac{S_j'}{S_j} \quad \text{and} \quad M_{22}^{(j)} = \frac{R_j'}{R_j}.$$

In all three cases: $M_{12}^{(j)} = M_{21}^{(j)} = 0$.

(3) Calculate the coefficients $\overline{M}_{kl}^{(i)}$:

$$\overline{M}_{kl}^{(i)} = \begin{cases} \frac{\tilde{\epsilon}_i\nu_{i-1}}{\tilde{\epsilon}_{i-1}\nu_i}M_{kl}^{(i)} & \text{for } k = 1, l = 1, 2 \\ \frac{\mu_i\nu_{i-1}}{\mu_{i-1}\nu_i}M_{kl}^{(i)} & \text{for } k = 2, l = 1, 2 \end{cases}$$

(4) Calculate the coefficients $L_{kl}^{(i)}$:

$$\begin{aligned} L_{11}^{(i)} &= S_i - \overline{M}_{11}^{(i+1)}R_i \\ L_{12}^{(i)} &= (\delta_i/\tilde{\epsilon_i} - \overline{M}_{12}^{(i+1)})R_i \\ L_{21}^{(i)} &= (\delta_i/\mu_i - \overline{M}_{21}^{(i+1)})R_i \\ L_{22}^{(i)} &= S_i - \overline{M}_{22}^{(i+1)}R_i \end{aligned}$$

and their derivatives $L_{kl}^{\prime(i)}$ by replacing in the upper equations R_i and S_i by $R_i^\prime$ and $S_i^\prime$, respectively. Here,

$$\delta_i = (\frac{\nu_i^2}{\nu_{i+1}^2} - 1)\frac{1}{\beta\nu_i a_i}.$$

(5) Calculate the coefficients $M_{kl}^{(i)}$:

$$\begin{aligned}
M_{11}^{(i)} &= \frac{1}{|\mathbf{L}|}(L_{11}^\prime L_{22} - L_{12}^\prime L_{21})^{(i)} \\
M_{12}^{(i)} &= \frac{1}{|\mathbf{L}|}(L_{12}^\prime L_{11} - L_{11}^\prime L_{12})^{(i)} \\
M_{21}^{(i)} &= \frac{1}{|\mathbf{L}|}(L_{21}^\prime L_{22} - L_{22}^\prime L_{21})^{(i)} \\
M_{22}^{(i)} &= \frac{1}{|\mathbf{L}|}(L_{22}^\prime L_{11} - L_{21}^\prime L_{12})^{(i)}
\end{aligned}$$

where $|\mathbf{L}| = (L_{11}L_{22} - L_{12}L_{21})^{(i)}$.
(6) Repeat steps (3) to (5) until $i = 3$ and compute $\overline{M}_{kl} := \overline{M}_{kl}^{(3)}$ from (3).
(7) Calculate the coefficients E_1 and H_1:

$$\begin{aligned}
E_1 &= \frac{\mathrm{i}\beta_1}{D}\left[(S_2 I_b^\prime + M R_2 I_b) - (\overline{M}_{11} R_2 I_b^\prime + \overline{M}_{22} S_2 I_b) + \frac{\gamma\beta_2 I_a}{\beta_1 kb}(\delta_2 - \overline{M}_{12})\right] \\
H_1 &= \frac{\mathrm{i}\beta_2}{D}\left[(S_2 I_b^\prime + M R_2 I_b) - (\overline{M}_{11} S_2 I_b + \overline{M}_{22} R_2 I_b^\prime) + \frac{\gamma\beta_1 I_a}{\beta_2 kb}(\delta_2 - \overline{M}_{21})\right]
\end{aligned}$$

with

$$\begin{aligned}
M &= \overline{M}_{11}\overline{M}_{22} - (\delta_2 - \overline{M}_{12})(\delta_2 - \overline{M}_{21}) \\
D &= I_b^{\prime 2} - (\overline{M}_{11} + \overline{M}_{22}) I_b I_b^\prime + M I_b^2 \\
\beta_1 &= 1 - \beta\beta_0 \\
\beta_2 &= \beta_0 - \beta
\end{aligned}$$

and where $I_a = I_1(ka/\gamma), I_b = I_1(kb/\gamma), I_b^\prime = I_1^\prime(kb/\gamma)$ and $a = a_1, b = a_2$.
(8) The transverse resistive wall impedance per unit length is then given by

$$\frac{Z_\perp}{L} = -\frac{\gamma^2}{\pi\epsilon_0 a^2 c\beta_0^2}[\mathrm{i}\beta_2^2 + I_a(\beta_1 E_1 + \beta_2 H_1)]$$

which also includes space charge effects.